

Quantized Hodgkin-Huxley Model for Quantum Neurons

Xiao-Hang Cheng,^{1,*} Tasio Gonzalez-Raya,^{2,*} Xi Chen,¹ Mikel Sanz,^{2,†} and Enrique Solano^{1,2,3}

¹*Department of Physics, Shanghai University, 200444 Shanghai, China*

²*Department of Physical Chemistry, University of the Basque Country UPV/EHU, Apartado 644, 48080 Bilbao, Spain*

³*IKERBASQUE, Basque Foundation for Science, Maria Diaz de Haro 3, 48013 Bilbao, Spain*

The Hodgkin-Huxley model describes the behavior of the membrane voltage in neurons, treating each element of the cell membrane as an electric circuit element, namely capacitors, memristors and voltage sources. We focus on the activation channel of potassium ions, since it is simpler, while keeping the majority of the features identified with the original Hodgkin-Huxley model. This simplification is physiologically meaningful, since it is related to some neurodegenerative and autoimmune diseases, which are associated with a process of demyelination in neurons. This model reduces to a memristor, a resistor whose resistance depends on the history of charges crossing it, coupled to a voltage source and a capacitor. Here, we take advantage of the recent quantization of the memristor to glance at the Hodgkin-Huxley model in the quantum regime. We compare the behavior of the potassium channel conductance in both the classical and quantum realm. In the latter, we firstly introduce classical sources to study the quantum-classical transition, and afterwards we switch to coherent quantum sources in order to study the effects of entanglement in the behavior of the quantum Hodgkin-Huxley model. Numerical simulations show an expected increment and adaptation depending on the history of signals in all regimes. Additionally, the response to AC sources showcases hysteretic behavior in the I-V characteristic curve due to the presence of the memristor. We investigate the memory capacitance represented by the area of the I-V loops, which we call memory persistence. We find that this memory persistence grows with entanglement, which can be interpreted in terms of the fundamental relation between information and thermodynamic entropies established by Landauer's principle. These results pave the way for the construction of quantum neuron networks inspired in the brain function but capable of dealing with quantum information. This could be considered a step forward towards the design of neuromorphic quantum architectures with direct implications in quantum machine learning.

I. INTRODUCTION

Brain science and neurophysiology are fascinating topics with deep questions and implications in the comprehension of the human being. Questions such as ‘How does brain work?’, ‘Can we utilize these functions to improve our life?’ catalyzed interdisciplinary research fields like biophysics and bioinformatics, among others. In 1963, the Nobel Prize in Physiology or Medicine was awarded to Alan Lloyd Hodgkin and Andrew Fielding Huxley for their work describing how electric signals in neurons propagates through the axon. They modelled it as an electric circuit represented by a set of non-linear differential equations [1], establishing a bridge between neuroscience and physics. Numerous researches about Hodgkin-Huxley’s neuron including noise sources have been published [2–9].

A neuron is an electrically excitable cell that receives, processes and transmits information through electrical signals, whose main components are the cell body, the dendrites and the axon. Dendrites are ramifications which receive and transmit stimulus into the cell body, which processes the signal. The nervous impulse is then propagated through the axon, which is an extension of

the nerve cell membrane. This propagation gradient is generated through the change in the ion permeabilities of the cell membrane when an impulse is transmitted. This implies a variation in ion concentrations represented in the Hodgkin-Huxley circuit by a non-linear conductance whose resistance depends on the history of electric charges crossing the cell, which is naturally identified with a memristor [10, 11].

In the last decade, we have witnessed a blossoming of quantum platforms and technologies. From the latter, Quantum Simulations, Quantum Detection and Quantum Communication are worth mentioning. Among quantum platforms, superconducting circuits stands out and currently shows the highest gradient in controllability, scalability and coherence. The combination of biosciences with quantum technologies from different perspectives gave birth to new research areas such as quantum biology [12, 13], quantum artificial life [14, 15] and quantum biomimetics [16], among others. In this framework, the merge of neurosciences and quantum technologies has also been considered, resulting, for instance, in the novel concept of neuromorphic quantum computing, in which brain-inspired architectures try to take advantage of entanglement to enhance computational power.

The recent proposal of the techniques for the quantization of the memristor [17], as well as its realization in both superconducting circuits [18] and integrated

* Both authors have contributed similarly to this work.

† mikel.sanz@ehu.eus

quantum photonics [19], allows for the construction of a quantized neuron model based on Hodgkin-Huxley's circuit. In the classical limit, this model reproduces the characteristic adaptive behaviour of brain neurons, whereas in the quantum regime it could unveil unique characteristics or an unprecedented learning performance. Furthermore, the study of coupled electric circuits containing memristors developed in recent years [20–22] sets an excellent starting position for the investigation of the dynamics of coupled quantum memristors for the construction of connected quantum neuron networks.

The idea of proposing mathematical models which condense the main features of real neurons is an old research area, and an attempt to extend it to the quantum realm has been launched in the recent past [23–28]. Furthermore, classical memristive devices have been used in the simulation of synaptic [29–31] as well as learning processes [32]. However, none of those works ever considered the Hodgkin-Huxley model with the quantum memristor.

In this article, we study a simplified version of the Hodgkin-Huxley model with biological interest, in which only the potassium ion channel plays a role. The ion conductance, modelled by a memristor, is coupled to a voltage source and a capacitor, studying its response under a periodic driving in both the classical and quantum regimes. Introducing a quantum memristor [17], we investigate the quantum regime with coherent state inputs by quantizing the elements in this circuit, comparing the membrane voltage, the conductance and the I-V characteristic curve for different input sources. Using the area of the hysteresis loop displayed in the I-V characteristic curve as a measure of the persistence of the memory [18, 19], we discover stronger memory effects in presence of entanglement: the higher the entanglement, the larger the hysteretic area. This can be explained due to the relation between information and thermodynamic entropies established through Landauer's principle, justifying why the hysteresis loop area, and therefore the energy dissipated, increases with the von Neumann entropy of the reduced states. This work establishes a roadmap for the construction of hardware-based quantum neuron networks enable to deal with quantum information, and the application to neuromorphic quantum architectures and quantum neural networks [33]. This could find applications in the field of quantum machine learning [34, 35] without the necessity of a universal quantum computer.

II. CLASSICAL HODGKIN-HUXLEY MODEL

The cell membrane of a neuron shows permeability changes for different ion species after the receiving electric impulses through the dendrites. These changes make possible variations on ion concentrations which, when overcoming a certain threshold, can lead to a sudden de-

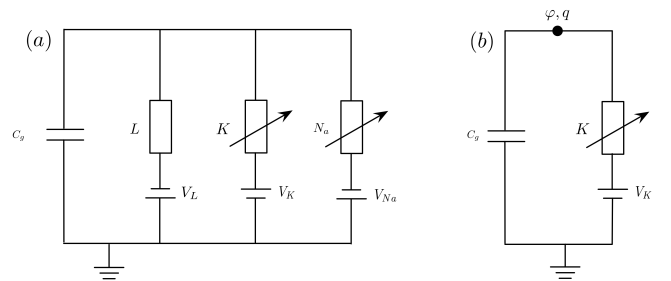


FIG. 1. (a) Hodgkin-Huxley circuit and (b) Hodgkin-Huxley circuit for a single potassium channel.

polarization of the membrane and the consequent transmission of the signal through the axon. These signals comprise mainly potassium and sodium ions, which have different roles during a potential spike. In 1952, Hodgkin and Huxley developed a model which describes the propagation of these stimuli by treating each component of the excitable cell membrane as an electric circuit element, as shown in Fig. 1 (a). The equations of this circuit are

$$I(t) = C_g \frac{dV_g}{dt} + \bar{g}_K n^4 (V_g - V_K) + \bar{g}_{N_a} m^3 h (V_g - V_{N_a}) + \bar{g}_L (V_g - V_L), \quad (1)$$

$$\frac{dn}{dt} = \alpha_n(V_g)(1 - n) - \beta_n(V_g)n, \quad (2)$$

$$\frac{dm}{dt} = \alpha_m(V_g)(1 - m) - \beta_m(V_g)m, \quad (3)$$

$$\frac{dh}{dt} = \alpha_h(V_g)(1 - h) - \beta_h(V_g)h, \quad (4)$$

where I is the total current, \bar{g}_i ($i = L, K, N_a$) is the maximum electrical conductance, C_g is the membrane capacitance, V_i is the equilibrium potential in each ion channel, and n, m, h are dimensionless quantities between 0 and 1 that represent the probability of activation or inactivation of each ion channel. Except for the leakage channel L , which accounts for small unperturbed flow of non-involved (mostly chloride) ions, and thus is described by a constant conductance, any ion channel is characterized by a non-linear conductance due to n, m and h , which weigh each channel differently and depend on voltage and time. Here, we keep solely the contribution coming from the potassium channel, which only has activation gates, and not both activation and inactivation gates as the sodium channel. This simplification is physiologically meaningful, since it is linked to some neurodegenerative and autoimmune diseases, which are associated with a process of demyelination in neurons. This model still conserves the most characteristic behavior of neurons. In this case, we are left with two coupled differential equations,

$$I(t) = C_g \frac{dV_g}{dt} + g_K n^4 (V_g - V_K), \quad (5)$$

$$\frac{dn}{dt} = \alpha_n(V_g)(1 - n) - \beta_n(V_g)n. \quad (6)$$

Naturally, this non-linear conductance can be identified with a memristor, which is a resistor whose resistance depends on the history of electrical signals, voltages or charges, crossing it [10]. It is the fourth basic element of electrical circuits, and introduces a relation between flux and charge. The equations describing the physical properties and memory effects of a (voltage-controlled) memristor are

$$I(t) = G(\mu(t))V(t), \quad (7)$$

$$\dot{\mu}(t) = f(\mu(t), V(t)), \quad (8)$$

where $G(\cdot)$ and $f(\cdot)$ are continuous real functions satisfying:

- (i) $G(\mu) \geq 0$ for all values of μ .
- (ii) For a fixed μ , $f(\mu, V)$ is monotone, and $f(\mu, 0) = 0$.

Property (i) ensures that the memristor is a passive element, and that $G(\mu)$ can indeed be understood as a conductance. Property (ii) restricts the internal variable dynamics to provide non-vanishing memory effects for all significant voltage inputs, implying that it does not have dynamics in the absence of voltage.

Notice that solving Eq. 8 requires time integration over the past of the control signal, and this solution affects $G(\mu)$. This means that the response in the current given by Eq. 7 depends not only on the present value of the control voltage, but also on the previous ones. Hence, if a memristor undergoes a periodic control signal, the I-V characteristic curve will display a hysteresis loop, which contains memory effects, identifying the slope of this curve with the resistance of the device.

The study of a single ion channel means neutralizing the dynamics of the other channel, which is a matter of controlling its voltage, namely its ionic concentration. Experimentally, an isolated study of the potassium channel goes through setting the membrane voltage to V_{Na} , or through changing the sodium concentration by replacing the sodic medium by any other non-gated substance. This was done in [1], and allowed them to obtain experimental results that could be compared to theoretical ones, thus testing the proposed expressions for α_x and β_x , with $x = n, m, h$ separately for each channel, so that values for n, m, h could be obtained. Then, with the conductance of the potassium channel given by $g_K = \bar{g}_K n^4$, Eqs. 5 and 6 can be solved numerically for the membrane voltage, given an input current $I(t)$.

III. QUANTUM HODGKIN-HUXLEY MODEL

In this section, we introduce a quantum version of the Hodgkin-Huxley model by quantizing each element of the circuit with one non-linear resistor, a voltage source and two capacitances. First, let us introduce the quantization of the memristor [17].

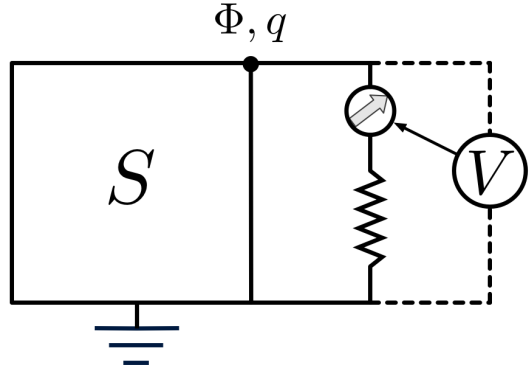


FIG. 2. Diagram of a quantum memristor as a resistor coupled to a closed system with a voltage-based weak-measurement scheme.

A. Quantum Memristor

We give a general description of the quantum memristor as a non-linear element in a closed circuit with a weak-measurement scheme, used to update the resistance. This layout can be seen in Fig. 2 as a closed system coupled to a resistor and a measurement apparatus, introducing a measurement-based update of the resistance depending on the voltage in the system.

The dynamics of the composite system can be studied by a master equation composed of a Hamiltonian part, a continuous-weak-measurement part and a classical feedback part,

$$d\rho = d\rho_H + d\rho_m + d\rho_d. \quad (9)$$

The Hamiltonian part is given by the von Neumann equation,

$$d\rho_H = -\frac{i}{\hbar}[H_S, \rho(t)]dt. \quad (10)$$

The continuous-weak-measurement part reads

$$d\rho_m = -\frac{\tau}{q_0^2}[q, [q, \rho(t)]]dt + \sqrt{\frac{2\tau}{q_0^2}(\{q, \rho(t)\} - 2\langle q \rangle \rho(t))}dW, \quad (11)$$

where the expectation value of an observable is $\langle A \rangle = \text{tr}(\rho A)$, τ is the projection frequency, q_0 is the uncertainty, and dW is the Wiener increment, associated to the stochasticity associated with weak measurements. The measurement strength is defined as $\kappa = \frac{\tau}{q_0^2}$.

The dissipation is described by Caldeira-Leggett master equation,

$$d\rho_d = -\frac{i\gamma(\mu)}{\hbar}[\varphi, \{q, \rho(t)\}]dt - \frac{2C\lambda\gamma(\mu)}{\hbar}[\varphi, [\varphi, \rho(t)]]dt \quad (12)$$

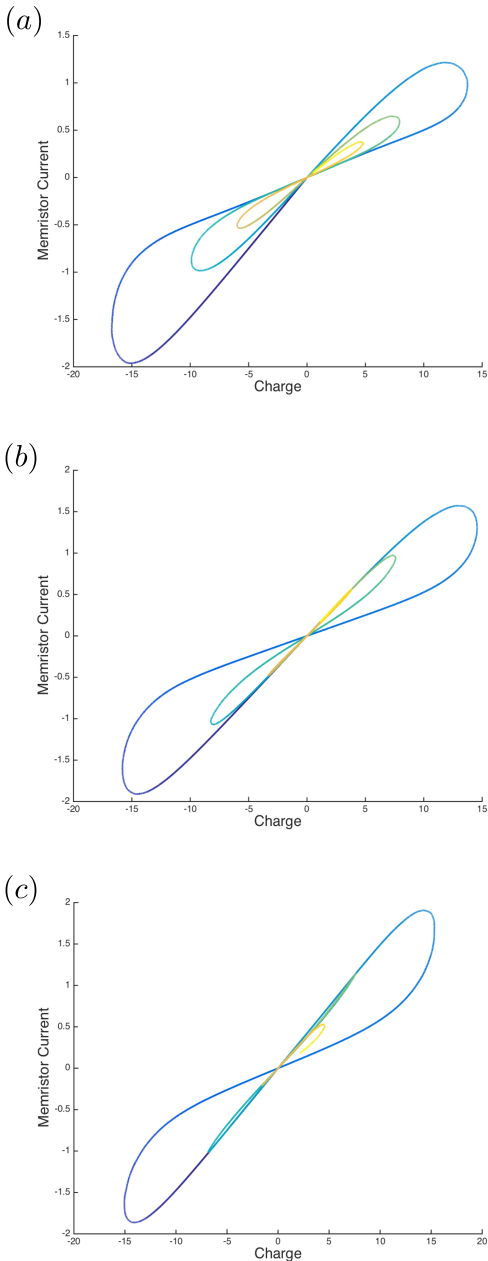


FIG. 3. Hysteresis loops a quantum memristor coupled to a LC circuit with a system Hamiltonian $H_S = \frac{q^2}{2C} + \frac{\phi^2}{2L}$, with $C = 1$ and $L = 1$ for different values of the voltage source: (a) $V = 0$, (b) $V = 0.5$, (c) $V = 1$, (d) $V = 2$

where $\lambda = k_B T / \hbar$ and $\gamma(\mu)$ is the dissipation function. Solving these equations we can have the relation between memristive current and the charge shown in Fig. 3, for an LC circuit coupled to a memristor, with a Hamiltonian of the form $H_S = \frac{q^2}{2C} + \frac{\phi^2}{2L}$. We can observe the memristor starts to show linearity in the hysteresis curves as we increase the voltage. In the case of a circuit with classical sources, or a circuit coupled to an open element, there is no need to introduce the Wiener noise.

B. Circuit Quantization

We proceed to study the quantization of the circuit shown in Fig. 4, for what we must obtain the Lagrangian. With a Hamiltonian formulation on sight, a description of electric circuits goes through defining fluxes and charges, from which the voltage and the current can be obtained by time differentiation. In this case we employ a node formulation, where node fluxes are the main variables and play the role of the spatial variable, with node charges being the conjugate variables. This formulation with node fluxes suffices to describe a circuit featuring linear capacitances and inductances.

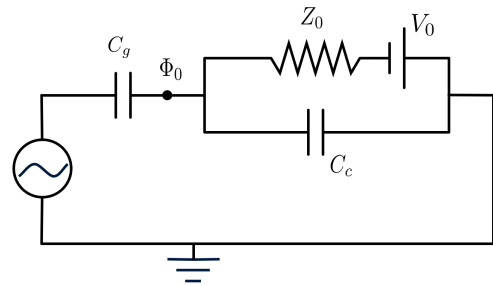


FIG. 4. Hodgkin-Huxley circuit for a single ion channel with a classical AC source $I(t) = I_0 \sin(\Omega t)$.

Although in the Lagrangian formalism dissipative elements such as resistors can be treated by means of adding a dissipation function to the equations of motion of an effective Lagrangian [36], the reversibility of the equivalent Hamilton equations coming from a Hamiltonian formulation needed for a proper circuit quantization, conflicts with the irreversibility of dissipative terms. A solution to this problem is to assume linear dissipation and treat the dissipative element in the Caldeira-Leggett model [37]. In this context, we just replace a linear dissipative element with a frequency-dependent impedance $Z(\omega)$ by an infinite set of coupled LC oscillators, i.e. a transmission line. The now infinite degrees of freedom of the resistor are identified with the intermediate node fluxes of the oscillators. This way we introduce the memristor as a linear dissipative element cast in the Caldeira-Leggett model.

The circuit can be seen in Fig. 5. We identify the impedance of the transmission line with the resistance of the memristor, and the impedance can be updated by hand, assuming that the time between two consecutive updates is much larger than the relaxation time of the memristor. The Lagrangian of this circuit can then be

written as

$$\mathcal{L} = \frac{C_c}{2} \dot{\Phi}_0^2 - \frac{(\Phi_1 - \Phi_0)^2}{2\Delta x L_0} + \left(\int_0^t dt' I(t') \right) \dot{\Phi}_0 + \sum_{i=1}^{\infty} \left[\frac{\Delta x C_0}{2} (\dot{\Phi}_i - V_0)^2 - \frac{(\Phi_{i+1} - \Phi_i)^2}{2\Delta x L_0} \right], \quad (13)$$

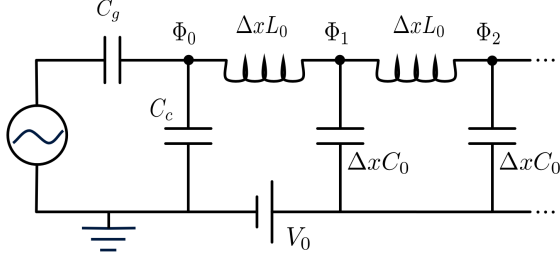


FIG. 5. Hodgkin-Huxley circuit for a single ion channel with a classical AC source $I(t) = I_0 \sin(\Omega t)$ effectively coupled to an infinite transmission line.

with C_0 and L_0 being the characteristic capacitance and impedance per unit length, respectively, of the transmission line. The equations of motion for $\Phi_0(x, t)$, which is the only quantum variable in this circuit and is related to the membrane voltage as $V_g(t) = -\dot{\Phi}_0(t)$, are obtained from the Euler-Lagrange equations, and by taking the continuum limit ($\Delta x \rightarrow 0$) we find

$$-\frac{1}{L_0} \frac{\partial \Phi_0}{\partial x} \Big|_{x=0} = C_c \ddot{\Phi}_0 \Big|_{x=0} + I(t) \quad (14)$$

In a circuit coupled to an infinite transmission line, the flux variables can be promoted onto a flux field at different spatial positions. The quantization of this field has been done, for example in [38], for infinite electrical networks, where can be found that

$$\Phi(x, t) = \sqrt{\frac{\hbar Z_0}{4\pi}} \int_0^\infty \frac{d\omega}{\sqrt{\omega}} (a_{in}(\omega) e^{-i(-k_\omega x + \omega t)} + a_{out}(\omega) e^{-i(k_\omega x + \omega t)} + H.c.), \quad (15)$$

where $k_\omega = |\omega| \sqrt{L_0 C_0}$ is the wave vector and $Z_0 = \sqrt{L_0/C_0}$ is the characteristic impedance of the transmission line, which we associate with the resistance of the memristor. By combining Eq. 14 with Eq. 16,

$$I(t) = -C_c \ddot{\Phi}_0 + \frac{1}{Z_0} (V_0 - \dot{\Phi}_0). \quad (16)$$

obtained from applying Kirchhoff's current laws to the circuit in Fig. 4, we can obtain expressions for the ingoing and outgoing annihilation operators $a_{in}(\omega)$ and $a_{out}(\omega)$, and thus solving Eq. 15 to obtain

$$\dot{\Phi}_0(t) = V_0 - \frac{I_0 Z_0}{2} \left[1 - \frac{\cos(2\Omega t) - 2C_c \Omega Z_0 \sin(2\Omega t)}{1 + 4C_c^2 \Omega^2 Z_0^2} \right] \quad (17)$$

We introduce an update for the resistance of the memristor by considering a time variation of Z_0 depending on the value of the membrane voltage. This approach is valid as long as the relaxation time of the set of LC circuits that models the memristor is much smaller than the time between successive measurements. Identifying the inverse of the impedance (admittance) with a conductance, we can use the equation $g_K(t) = \bar{g}_K n(t)^4$ of the potassium channel conductance to update the impedance as $Z(t) = Z_{min} n(t)^{-4}$, with Eq. 6, such that

$$\dot{Z}(t) = -4Z_{min} \left(\frac{Z(t)}{Z_{min}} \right)^{5/4} \alpha(V_g) + 4Z(t)(\alpha(V_g) + \beta(V_g)), \quad (18)$$

Thus, from now on we identify the potassium channel conductance with the inverse of the impedance of the transmission line.

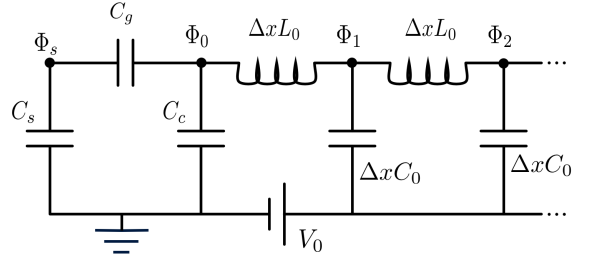


FIG. 6. Hodgkin-Huxley circuit for a single ion channel with a coherent state source, $\alpha(t) = \alpha_0 \sin(\Omega t)$, effectively coupled to an infinite transmission line.

So far we have studied a quantum version of the Hodgkin-Huxley model under a classical AC source, but we want to test this model for different kinds of coherent state inputs. For this we introduce a new node flux, $\Phi_s = (\Phi_s^{(1)} + \Phi_s^{(2)})/2$, with $\Phi_s^{(i)} = \sqrt{\frac{\hbar}{2\Omega C_s}} (a_i + a_i^\dagger)$, to replace the classical source. By averaging Φ_s over the input states, we can effectively quantize the source. This new circuit is shown in Fig. 6, and its Lagrangian can be written as

$$\mathcal{L} = \frac{C_s}{2} \dot{\Phi}_s^2 + \frac{C_g}{2} (\dot{\Phi}_s - \dot{\Phi}_0)^2 + \frac{C_c}{2} \dot{\Phi}_0^2 - \frac{(\Phi_1 - \Phi_0)^2}{2\Delta x L_0} + \sum_{i=1}^{\infty} \left[\frac{\Delta x}{2} (\dot{\Phi}_i - V_0)^2 - \frac{(\Phi_{i+1} - \Phi_i)^2}{2\Delta x L_0} \right], \quad (19)$$

where the equation of motion for $\Phi_0(x, t)$ is

$$-\frac{1}{L_0} \frac{\partial \Phi_0}{\partial x} \Big|_{x=0} = -C_g (\dot{\Phi}_s - \dot{\Phi}_0) \Big|_{x=0} + C_c \ddot{\Phi}_0 \Big|_{x=0} \quad (20)$$

In this equation, $-C_g \langle \dot{\Phi}_s \rangle_s$ averaged over some state $|s\rangle$ plays the role of the source. For a coherent state input

$|s\rangle = |\alpha\rangle$ with $\alpha = \alpha_0 \sin(\Omega t)$ the input current is

$$I(t) = -C_g \langle \ddot{\Phi}_s \rangle_s = \frac{\alpha_0 C_g \omega^2}{2} \sqrt{\frac{\hbar}{2\Omega C_s}} \sin(\Omega t). \quad (21)$$

Following the previous procedure to find the voltage,

$$\begin{aligned} \dot{\Phi}_0(t) &= V_0 + \\ &+ \frac{\alpha_0 C_g \Omega^2 Z_0}{2\sqrt{2C_s \Omega}} \left[\frac{(C_g + C_c)\Omega Z_0 \cos(\Omega t) + \sin(\Omega t)}{1 + (C_c + C_g)^2 \Omega^2 Z_0^2} \right]. \end{aligned} \quad (22)$$

For an entangled state $|s\rangle = \cos \theta |\alpha, 0\rangle + \sin \theta |0, \alpha\rangle$, the input source corresponds to

$$I(t) = \frac{\alpha_0 C_g \omega^2}{2} \sqrt{\frac{\hbar}{2\Omega C_s}} \sin(\Omega t) (1 + \sin(2\theta) e^{-\frac{|\alpha_0|^2}{2} \sin^2(\Omega t)}), \quad (23)$$

which does not have a Fourier transform to frequency space. Then, we need to make an approximation, such that

$$\begin{aligned} \sin(\Omega t) (1 + \sin(2\theta) e^{-\frac{|\alpha_0|^2}{2} \sin^2(\Omega t)}) &\simeq \\ \sin(\Omega t) \left[1 + \sin(2\theta) \left(1 - \frac{|\alpha_0|^2}{2} \sin^2(\Omega t) - \frac{|\alpha_0|^4}{4} \sin^4(\Omega t) + \right. \right. \\ \left. \left. + \frac{|\alpha_0|^6}{12} \sin^6(\Omega t) - \frac{|\alpha_0|^8}{48} \sin^8(\Omega t) \right) \right] \end{aligned} \quad (24)$$

For simplicity, we just take α_0 to be real. This way we find the voltage to be

$$\begin{aligned} \dot{\Phi}_0(t) = &V_0 + \frac{\alpha_0 C_g \Omega^2 Z_0}{24576 \sqrt{2C_s \Omega}} \left\{ 2(6144 + (6144 - 3204\alpha_0^2 + 960\alpha_0^4 - 280\alpha_0^6 + 63\alpha_0^8) \sin(2\theta)) \left[\frac{\sin(\Omega t) + (C_g + C_c)\Omega Z_0 \cos(\Omega t)}{1 + (C_g + C_c)^2 \Omega^2 Z_0^2} \right] + \right. \\ &\sin(2\theta) \alpha_0^2 \left[108(128 - 80\alpha_0^2 + 28\alpha_0^4 - 7\alpha_0^6) \left[\frac{\sin(3\Omega t) + 3(C_g + C_c)\Omega Z_0 \cos(3\Omega t)}{1 + 9(C_g + C_c)^2 \Omega^2 Z_0^2} \right] + \right. \\ &100\alpha_0^2(48 - 28\alpha_0^2 + 9\alpha_0^4) \left[\frac{\sin(5\Omega t) + 5(C_g + C_c)\Omega Z_0 \cos(5\Omega t)}{1 + 25(C_g + C_c)^2 \Omega^2 Z_0^2} \right] + \\ &49\alpha_0^4(16 - 9\alpha_0^2) \left[\frac{\sin(7\Omega t) + 7(C_g + C_c)\Omega Z_0 \cos(7\Omega t)}{1 + 49(C_g + C_c)^2 \Omega^2 Z_0^2} \right] + 81\alpha_0^6 \left[\frac{\sin(9\Omega t) + 9(C_g + C_c)\Omega Z_0 \cos(9\Omega t)}{1 + 81(C_g + C_c)^2 \Omega^2 Z_0^2} \right] \left. \right] \left. \right\}. \end{aligned} \quad (25)$$

With a different dependence of the voltage on Z_0 , we can again solve Eq. 18 numerically to obtain the impedance of the memristor, from which we can compute the potassium channel conductance, and the membrane voltage. Another interesting thing to obtain is the area of the hysteresis loop that is formed when the membrane voltage is plotted versus the input current as the I-V characteristic curve, as it has been proposed as a natural measure of the persistence of the memory in the memristor. Through Landauer's principle we can establish a connection between thermodynamic entropy, related to dissipation, and thus related to the area of the hysteresis loop, and information entropy, by computing the von Neumann entropy of the reduced input states, which can be used as a measure of entanglement, to illustrate the presence of memory effects with the use of entangled states.

IV. RESULTS

In this section we present the results for the membrane voltage and for the conductance of the potassium channel in four different scenarios: the classical Hodgkin-Huxley model, the quantum Hodgkin-Huxley model with a classi-

cal AC source, the quantum Hodgkin-Huxley model with a coherent state input and the quantum Hodgkin-Huxley model with an entangled coherent state input. We also compute the area of the hysteresis loop, and the von Neumann entropy, as a comparison to see memory improvements with the use of different inputs.

A. Classical Hodgkin-Huxley model

We solve Eqs. 5 and 6 and plot the membrane voltage for a periodic input current of the form $I(t) = I_0 \sin^2(\Omega t)$, taking the membrane voltage to be initially zero. The result of the membrane voltage plotted over time can be seen as the blue curve in Fig. 8. We can observe an initial spike in the voltage, followed by a quick relaxation. This might seem odd, as we are only dealing with one ion channel, but the values for the coefficients $\alpha(V_g)$ and $\beta(V_g)$ were obtained experimentally [1], so the gate-opening probability n is not completely independent of m and h .

Comparing the conductance in Fig. 8 (red curve) with the one in [1], we see a short initial delay of the increase

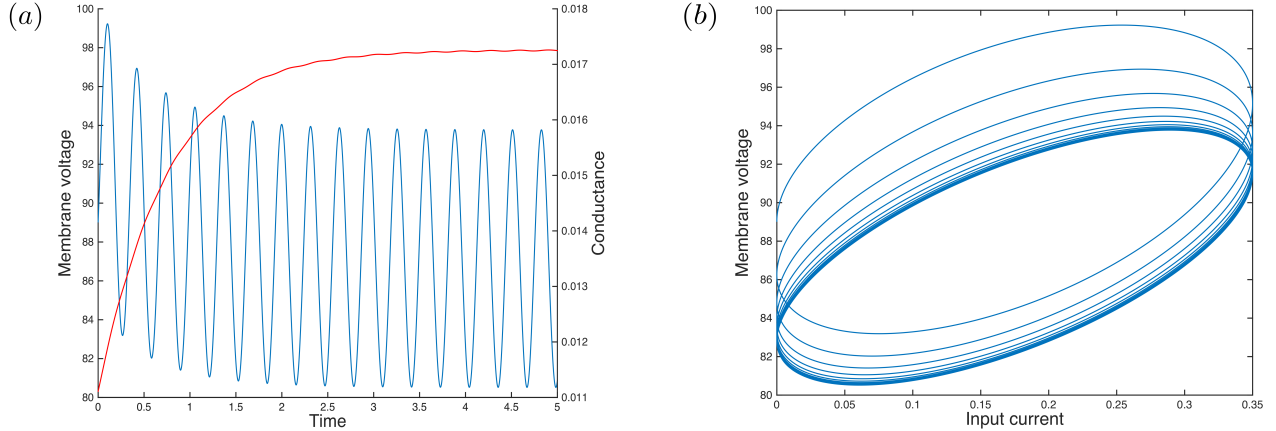


FIG. 7. Quantum Hodgkin-Huxley model with a classical periodic input $I(t) = I_0 \sin^2(\Omega t)$: (a) Membrane voltage (blue) and potassium conductance (red) over time. (b) Membrane voltage versus input current.

with oscillations caused by our choice of $I(t)$ and an eventual relaxation. We appreciate that with the introduction of an input signal the conductance rises and adapts to this signal, according to the depolarization of the membrane.

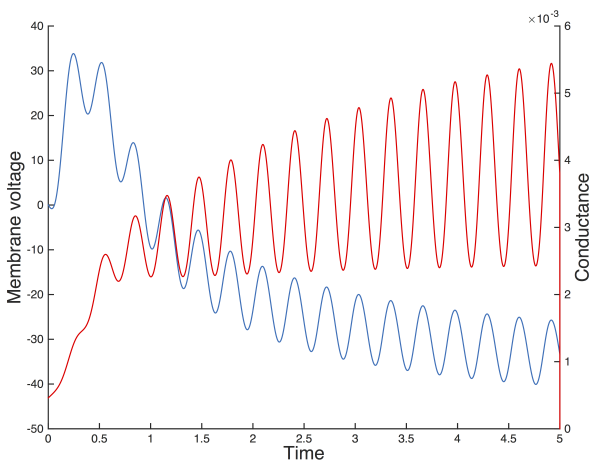


FIG. 8. Membrane voltage (blue) and potassium conductance (red) over time in the classical Hodgkin-Huxley model with a periodic input.

B. Quantum Hodgkin-Huxley model with classical input

Solving Eqs. 17 and 18 we obtain the membrane voltage and the potassium conductance in the quantum model with a classical input $I(t) = I_0 \sin^2(\Omega t)$. The membrane voltage plotted over time can be seen as the blue curve in Fig. 7 (a). We can observe a small spike in the voltage, as it quickly adapts to the input.

The conductance in Fig. 7 (a) (red curve) does not feature the desired delay in its growth, but its saturation is more clear, and although it saturates fast, it starts to resemble the desired s-shaped curve displayed by the saturation of the potassium conductance in [1]. The dependence of these functions on the initial values of the impedance and on I_0 is expectable, as we are dealing with a non-linear element in our circuit.

We introduce the I-V characteristic curve as we plot the membrane voltage versus the input current, shown in Fig. 7 (b), featuring a memristive hysteresis loop. The shape of this curve depends on the initial conditions, as initial values further away from the maximal value of the impedance will cause the system to have a longer saturation time. However, the system eventually relaxes into a limit cycle, which is independent of the initial conditions.

C. Quantum Hodgkin-Huxley model with coherent state input

Solving Eqs. 18 and 22 with a coherent state input of $\alpha(t) = \alpha_0 \sin(\Omega t)$, we obtain the membrane voltage and the potassium conductance, shown in Fig. 9 (a) as the blue curve and the red curve, respectively. We do not observe a spike in the voltage, but quite a slow decrease in the oscillation amplitude. The conductance in Fig. 9 (a) features a noticeable delay of the growth, and its form gets closer to a s-shaped curve resulting from a rise in conductance with an adaptation when an input is introduced.

The hysteresis loop of the memristor, shown in Fig. 9 (b) is now shaped differently, due to the change from $\sin^2(\Omega t)$ to $\sin(\Omega t)$ on the input. In this case, it can be appreciated that trajectories shrink into a limit cycle.

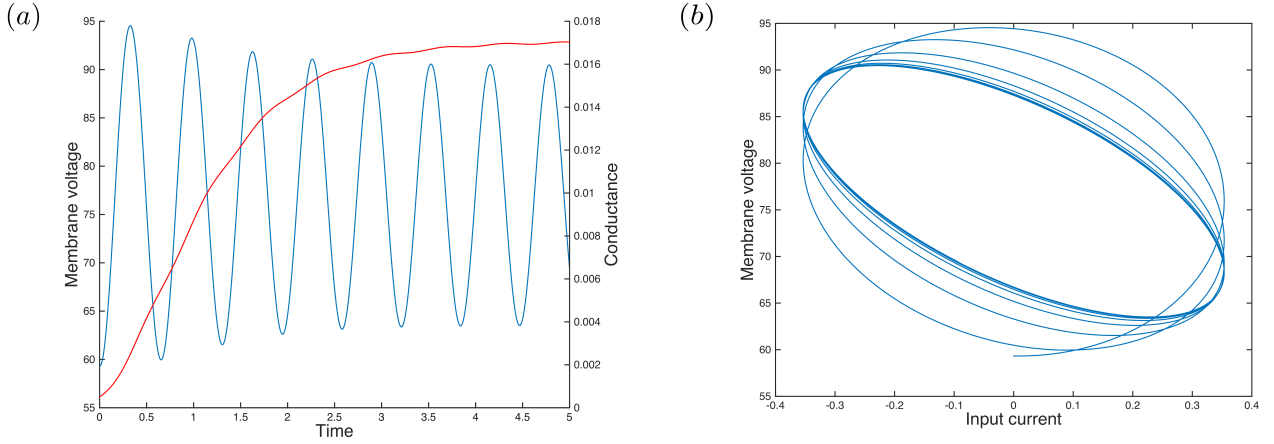


FIG. 9. Quantum Hodgkin-Huxley model with coherent state input $\alpha(t) = \alpha_0 \sin(\Omega t)$: (a) Membrane voltage (blue) and potassium conductance (red) over time. (b) Membrane voltage versus input current.

D. Quantum Hodgkin-Huxley model with entangled coherent state input

The last instance of this quantum Hodgkin-Huxley model goes through studying the system for an input of entangled coherent states, $|s\rangle = \cos\theta|\alpha, 0\rangle + \sin\theta|0, \alpha\rangle$, with $\alpha(t) = \alpha_0 \sin(\Omega t)$. Notice that this state is not properly normalized in the cases when $\sin(\Omega t) = 0$. Solving Eqs. 18 and 25, we plot the membrane voltage (in blue) and the potassium conductance (in red) over time in Fig. 12 (a). Again, there is not a clear spike, but we observe initial oscillations that more obviously decrease in amplitude. The conductance in Fig. 12 (a) also features the s-shape in its growth, and in fact is very similar to the one obtained with a coherent state input, although oscillations are more present in this case due to numerical noise.

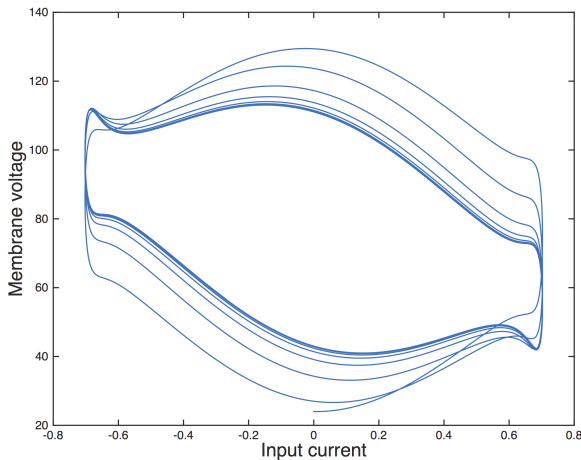


FIG. 10. Membrane voltage versus entangled coherent state input current with $\alpha_0 = 1.5$, giving a hysteresis loop.

The hysteresis loop of the memristor, shown in Fig. 12 (b), is similar to the one of the coherent state input, where the curves shrink into a limit cycle. These results have been obtained for a choice of $\alpha_0 = 1$, whereas figures 10 and 11 illustrate how the shape of the hysteresis loop changes with the α_0 , such that an increase in α_0 goes along with an increase in the memristive area. We can see that a slight modification on the amplitude of the input has a big impact on the shape of the hysteresis loop, which is a sign of non-linear behavior.

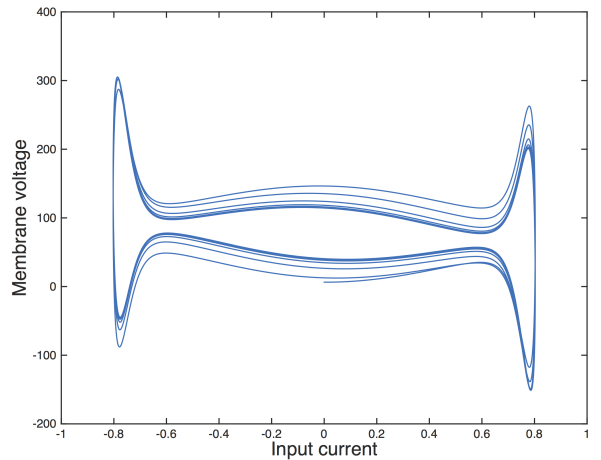


FIG. 11. Membrane voltage versus entangled coherent state input with $\alpha_0 = 2$, giving a hysteresis loop.

E. Memory

We compare the area of the hysteresis loop for different inputs, as shown in Table I (a). The premise of this comparison is that the larger the area, the greater

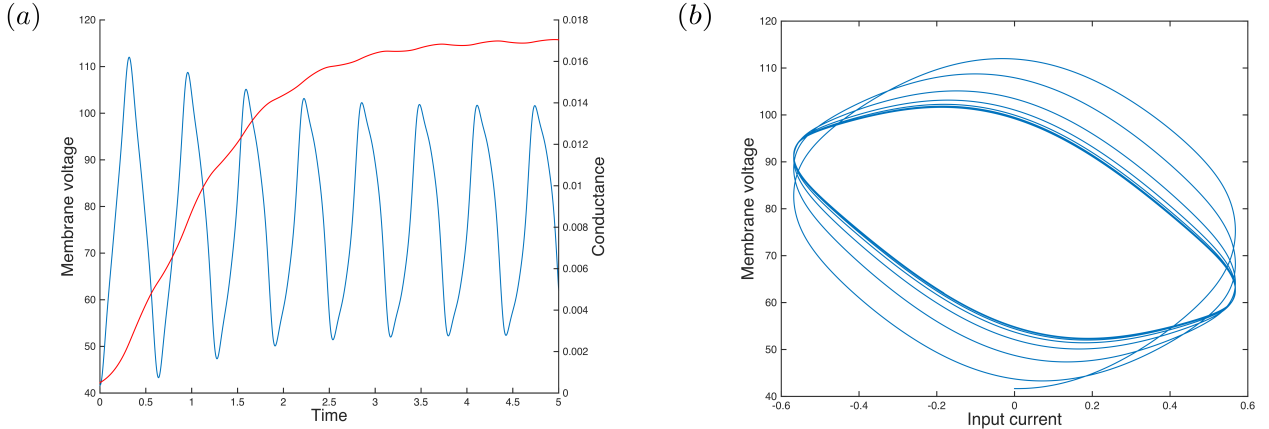


FIG. 12. Quantum Hodgkin-Huxley model with entangled coherent state input $|s\rangle = \cos\theta|\alpha, 0\rangle + \sin\theta|0, \alpha\rangle$: (a) Membrane voltage (blue) and potassium conductance (red) over time. (b) Membrane voltage versus input current.

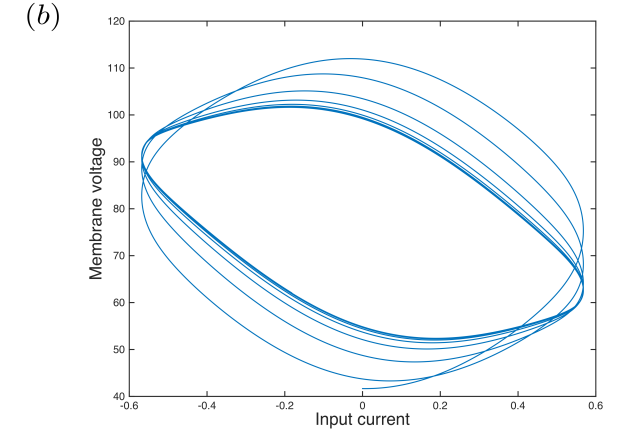
the memory persistence. The measures of the area of hysteresis loops grow as presented in Table I (a), reaching a maximum value for the instance of an entangled state input. This illustrates that the introduction of a quantum version of the Hodgkin-Huxley model with quantum inputs represents an improvement in the persistence of the memory. One reason for this marked increase in area is the change in the driving of the input current, from $\sin(\Omega t)^2$ in models A and B using a classical source, to $\sin(\Omega t)$ in models C and D using a quantum source, referring to the subsections in this presentation of the results. Even so, in the latter we still observe a rise in area due to the use of entangled states.

(a)	Model	A	B	C	D ₀	D _{$\pi/4$}
	Area	21.83	60.96	102.32	102.32	157.75

(b)	θ	α_0	Area	α_0	Area	α_0	Area
	0	1	102.32	1.5	148.93	2	192.54
	$\pi/6$	1	150.60	1.5	184.13	2	211.20
	$\pi/4$	1	157.75	1.5	189.42	2	215.03
	1	1	152.92	1.5	185.85	2	212.40
	$5\pi/12$	1	130.63	1.5	169.47	2	202.15

TABLE I. (a) Area of the hysteresis loop for the previously discussed models. (b) Area of the hysteresis loop in the quantum Hodgkin-Huxley model with entangled coherent state input $\cos\theta|\alpha, 0\rangle + \sin\theta|0, \alpha\rangle$ for different values of θ and α_0 .

In Table I (b) we observe how the area of the memristive curve obtained with an entangled state input changes with the variation of parameters such as α_0 and θ . The area of the hysteresis loop increases with α_0 , so the memory persistence is improved with an increase in the amplitude of the input signal. $\theta = \pi/4$ corresponds to a maximally entangled state, for which the memory effects are larger, whereas the lowest value of the area comes for $\theta = 0$, for which the state is not entangled.



To illustrate these statements, we can use the von Neumann entropy as an indication of how entangled a quantum state is and how it can be related to memory. This is done by taking the partial trace of $\rho = |s\rangle\langle s|$ over any of the two subsystems, resulting in a reduced state state, as $\rho_1 = \text{tr}_2 |s\rangle\langle s|$, and computing the von Neumann entropy of this state, $S = -\text{tr}[\rho_1 \ln \rho_1]$. This result is plotted for different values of $\theta \in [0, \pi/4]$ in Fig 13.

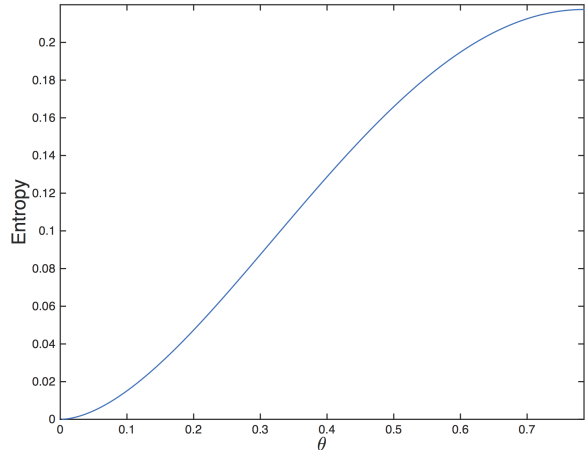


FIG. 13. Von Neumann entropy of the reduced state ρ_1 in terms of θ , between $\theta = 0$ (not entangled) and $\theta = \pi/4$ (maximally entangled).

This entropy can be used as a measure of memory because entangled states carry information in their entanglement, and when the partial trace is taken over an entangled state, it loses this information, i.e. becomes a mixed state. Taking the partial trace over a maximally entangled state gives a maximally mixed state, i.e. $1/d$, where d is the dimension of our space, and the entropy of a maximally mixed state is maximal,

$S = \ln d$. On the contrary, when we have a pure state, such as $|\alpha, 0\rangle$ or $|0, \alpha\rangle$, the entropy is zero.

The von Neumann entropy is the quantum equivalent of the Shannon entropy, which is not a thermodynamical entropy, but describes information. It can be interpreted as a measure of how much information is encoded in a quantum state. Thus, it is another way of measuring the memory, the other one being of course the area of the hysteresis loop.

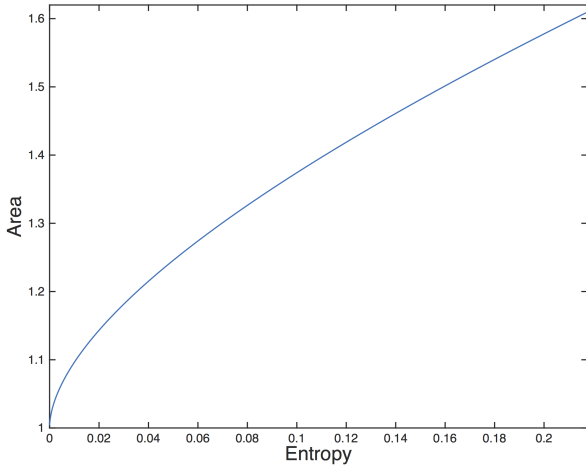


FIG. 14. Area of the hysteresis loop related to an entangled state input divided by the one related to a coherent state input in terms of the von Neumann entropy.

Hysteresis implies irreversible thermodynamic change, thus implying dissipation. Landauer's principle establishes a relation between entropy in thermodynamics and in information theory, such that any process involving a manipulation of physical information implies an increase in entropy, i.e. dissipation. The larger the area of the hysteresis loop, the larger the energy dissipated, which corresponds to a larger loss of information, implying a larger entropy. A relation between von Neumann entropy and hysteresis area, as can be seen in Fig 14. As expected, an increase in the von Neumann entropy is followed by an increase in the memristive area, both reaching a maximal value for maximally entangled states ($\theta = \pi/4$).

V. CONCLUSIONS & OUTLOOK

We have studied a simplified version of the Hodgkin-Huxley model with a single ion channel as a circuit featuring a capacitance, a voltage source and a memristor under a periodic input in the classical regime, and under coherent state inputs in the quantum regime by introducing the quantum memristor. Then we compared the membrane voltage, the potassium conductance and

the I-V characteristic curve in both regimes, and from the former one we extracted useful information related to the system's memory persistence by looking at the area of the hysteresis loop.

This work shows that the behavior of this simplified version of the classical Hodgkin-Huxley model can be reproduced in the quantum regime, with the spike in the membrane voltage replaced by a slow relaxation. The conductance showed good results according to the experiments carried out in Ref. [1], rising as an s-shaped curve, result of a displacement from a resting value by an input source with an eventual adaptation, unaffected by intermediate and relaxation oscillations. This saturation or adaptation is identified with a learning process by the memristive device.

Beyond this simplified model, a study of the two-ion channel Hodgkin-Huxley model in the quantum regime, which amounts to add a second memristor corresponding to the conductance of the sodium channel, would unveil new characteristics of the mechanism that rules the transmission of nervous impulses in neurons. For example, we expect to see an initial spike in the sodium conductance, knowing that the mechanism of the sodium channel consists of a fast activation gate followed by inactivation. But this work would also carry a complete new result of a different kind: the dynamics of two quantum memristors connected in parallel have never been studied.

The main result of this paper is the discovery that maximal values of the area of the memristive curves correspond to the use of entangled coherent state inputs, meaning greater memory persistence. Similar results were obtained when looking at the von Neumann entropy of the reduced states, then finding that an increase in this entropy was followed by an increase in the area. Thus, this establishes a connection between two measures of memory effects, one from thermodynamics based on dissipation, and one from information theory, based on entanglement. Given that entangled states are genuinely quantum, this result lays the foundations for future research on quantum neurons with quantum state inputs. Memory effects are more relevant when displayed in connected neuron networks, studying the output of a string of neurons with an entangled state input, which would imply yet another novel discovery: the dynamics of two serially-connected circuits featuring quantum memristors have never been studied either.

The answer to these two questions can set excellent starting points for any advances in neuromorphic quantum computing and neural networks, with direct implications on machine learning.

ACKNOWLEDGEMENT

The authors acknowledge support from NSFC (11474193), the Shuguang (14SG35), the program of Shanghai Municipal Science and Technology Commission (18010500400 and 18ZR1415500), Spanish

MINECO/FEDER FIS2015-69983-P and Basque Government IT986-16. This material is also based upon work supported by the U.S. Department of Energy, Office of Science, Office of Advance Scientific Computing Research (ASCR), under field work proposal number ERKJ335.

-
- [1] A. L. Hodgkin and A. F. Huxley, “A quantitative description of membrane current and its application to conduction and excitation in nerve”, *J. Physiol.* **117**, 500-544 (1952).
 - [2] S.-G. Lee, A. Neiman, and S. Kim, “Coherence resonance in a Hodgkin-Huxley neuron”, *Phys. Rev. E* **57**, 3292 (1998).
 - [3] Y.-Q. Wang, David T. W. Chik, and Z. D. Wang, “Coherence resonance and noise-induced synchronization in globally coupled Hodgkin-Huxley neurons”, *Phys. Rev. E* **61**, 740 (2000).
 - [4] C. Zhou and J. Kurths, “Noise-induced synchronization and coherence resonance of a Hodgkin-Huxley model of thermally sensitive neurons”, *Chaos An Interdisciplinary Journal of Nonlinear Science* **13**, 401 (2003).
 - [5] L. A. da Silva and R. D. Vilela, “Colored noise and memory effects on formal spiking neuron models”, *Phys. Rev. E* **91**, 062702 (2015).
 - [6] E. Yilmaza, V. Baysala, and M. Ozer, “Enhancement of temporal coherence via time-periodic coupling strength in a scale-free network of stochastic Hodgkin-Huxley neurons”, *Phys. Lett. A* **379**, 1594 (2015).
 - [7] X.-M. Guo, J. Wang, J. Liu, H.-T. Yu, and R. F. Galán, “Optimal time scales of input fluctuations for spiking coherence and reliability in stochastic Hodgkin-Huxley neurons”, *Physica A* **468**, 381-390 (2017).
 - [8] H.-T. Yu, R. F. Galán, J. Wang, Y.-B. Cao, and J. Liu, “Stochastic resonance, coherence resonance, and spike timing reliability of Hodgkin-Huxley neurons with ion-channel noise”, *Physica A* **471**, 263-275 (2017).
 - [9] Y.-H. Hao, Y.-B. Gong, X. Lin, Y.-H. Xie, and X.-G. Ma, “Transition and enhancement of synchronization by time delays in stochastic Hodgkin-Huxley neuron networks”, *Neurocomputing*, **73**, 2998-3004 (2010).
 - [10] L. O. Chua, “Memristor-The missing circuit element”, *IEEE Trans. Circuit Theory* **18**, 507-519 (1971).
 - [11] L. O. Chua and S. M. Kang, “Memristive devices and systems”, *Proc. IEEE* **64**, 209 (1976).
 - [12] M. Mohseni, P. Rebentrost, S. Lloyd, and A. Aspuru-Guzik, “Environment-assisted quantum walks in photosynthetic energy transfer”, *J. Chem. Phys.* **129**, 174106 (2008).
 - [13] M. Mohseni, Y. Omar, G. S. Engel, and M. B. Plenio, “Quantum effects in biology”, Cambridge University Press, Cambridge (2014).
 - [14] U. Alvarez-Rodriguez, M. Sanz, L. Lamata, and E. Solano, “Artificial Life in Quantum Technologies”, *Sci. Rep.* **6**, 20956 (2016).
 - [15] U. Alvarez-Rodriguez, M. Sanz, L. Lamata, and E. Solano, “Quantum Artificial Life in an IBM Quantum Computer”, arXiv:1711.09442 (2017).
 - [16] U. Alvarez-Rodriguez, M. Sanz, L. Lamata, and E. Solano, “Biomimetic Cloning of Quantum Observables”, *Sci. Rep.* **4**, 4910 (2014).
 - [17] P. Pfeiffer, I. L. Egusquiza, M. Di Ventra, M. Sanz, and E. Solano, “Quantum Memristor”, *Sci. Rep.* **6**, 29507 (2016).
 - [18] J. Salmilehto, F. Deppe, M. Di Ventra, M. Sanz, and E. Solano, “Quantum Memristors with Superconducting Circuits”, *Sci. Rep.* **7**, 42044 (2017).
 - [19] M. Sanz, L. Lamata, and E. Solano, “Quantum Memristors in Quantum Photonics”, *APL Photonics* **3**, 080801 (2018).
 - [20] D. Yu, H. H.-C. Iu, Y. Liang, T. Fernando, and L. O. Chua, “Dynamic Behavior of Coupled Memristor Circuits”, *IEEE Trans. Circuits and Systems I: Regular Papers* **62**, 1607-1616 (2015).
 - [21] R. K. Budhathoki, M. Pd. Sah, S. P. Adhikari, H. Kim, and L. O. Chua, “Composite Behavior of Multiple Memristor Circuits”, *IEEE Trans. Circuits and Systems I: Regular Papers* **60**, 2688-2700 (2013).
 - [22] L. O. Chua, “Resistance Switching Memories are Memristors”, *Applied Physics A* **102**, 765-783 (2011).
 - [23] N. Gomez, J. O. Winter, F. Shieh, A. E. Saunders, B. A. Korgel, and C. E. Schmidt, “Challenges in quantum dot-neuron active interfacing”, *Talanta*, **67**, 462-471 (2005).
 - [24] M. Maeda, M. Suenaga, and H. Miyajima, “Qubit neuron according to quantum circuit for XOR problem”, *Appl. Math. Comput.* **185**, 1015-1025 (2007).
 - [25] Michail Zak, “From quantum entanglement to mirror neuron”, *Chaos*, **34**, 344-359 (2007).
 - [26] D. Ventura and T. Martinez, “An Artificial Neuron with Quantum Mechanical Properties”. *Artificial Neural Nets and Genetic Algorithms.*, Springer, Vienna (1998).
 - [27] Y.-D. Cao, G. G. Guerreschi, and A. Aspuru-Guzik, “Quantum Neuron: an elementary building block for machine learning on quantum computers”, arXiv:1711.11240 (2017).
 - [28] N. Kouda, N. Matsui, and H. Nishimura, “Learning performance of neuron model based on quantum superposition”, *IEEE RO-MAN*, 112-117 (2000).
 - [29] G. S. Snider *et al.*, “From synapses to circuitry: Using memristive memory to explore the electronic brain”, *Computer* **44**, 21 (2011).
 - [30] R. Berdan, E. Vasilaki, A. Khiat, G. Indiveri, A. Serb, and T. Prodromakis, “Emulating short-term synaptic dynamics with memristive devices”, *Sci. Rep.* **6**, 18639 (2015).
 - [31] Y. V. Pershin and M. Di Ventra, “Neuromorphic, Digital, and Quantum Computation with Memory Circuit Elements”, *Proc. IEEE* **100**, 2071-2080 (2012).
 - [32] T. Serrano-Gotarredona, T. Masquelier, T. Prodromakis, G. Indiveri, and B. Linares-Barranco, “STDP and STDP variations with memristors for spiking neuromorphic learning systems”, *Front. Neurosci.* **7**, 2 (2013).

- [33] F. Silva, M. Sanz, J. Seixas, E. Solano, and Y. Omar, “Perceptrons from Memristors”, arXiv:1807.04912 (2018).
- [34] M. Schuld, I. Sinayskiy, and F. Petruccione, “An introduction to quantum machine learning”, *Contemp. Phys.* **56**, 172-185 (2015).
- [35] J. Biamonte, P. Wittek, N. Pancotti, P. Rebentrost, N. Wiebe, and S. Lloyd, “Quantum Machine Learning”, *Nature* **549**, 195 (2017).
- [36] G. Z. Cohen, Y. V. Pershin, and M. Di Ventra, “Lagrange Formalism of Memory Circuit Elements: Classical and Quantum Formulation”, *Phys. Rev. B* **85**, 165428 (2012).
- [37] U. Vool and M. Devoret, “Introduction to Quantum Electromagnetic Circuits”, *Int. J. Circuit Theory and Applications* **45**, 897-934 (2016).
- [38] B. Yurke and J. S. Denker “Quantum Network Theory”, *Phys. Rev. A* **29**, 1419 (1984).